Review

For reprint orders, please contact: reprints@futuremedicine.com

Nanomedicine

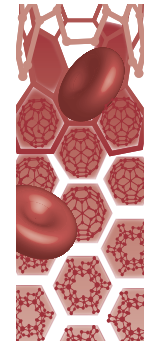

Putting gold nanocages to work for optical imaging, controlled release and cancer theranostics

Gold nanocages are hollow nanostructures with ultrathin, porous walls. They are bioinert and their surface can be readily modified with functional groups to specifically interact with the biological system of interest. They have remarkable optical properties, including localized surface plasmon resonance peaks tunable to the near-infrared region, strong absorption and scattering, as well as two- and three-photon luminescence. With the establishment of robust protocols for both synthesis and surface functionalization, Au nanocages have been extensively explored for various biomedical applications. In this review, we begin with a brief account of the synthesis and properties of Au nanocages, and then highlight some of the recent developments in applying them to an array of biomedical applications related to optical imaging, controlled release and cancer theranostics.

First draft submitted: 15 March 2016; Accepted for publication: 3 May 2016; Published online: 27 June 2016

Keywords: cancer theranostics • controlled release • gold nanostructures • hollow nanostructures • nanocages • near-infrared • optical imaging • plasmonics

Bo Pang[1,2], Xuan Yang[1] & Younan Xia*[,1,3]

[1]The Wallace H. Coulter Department of Biomedical Engineering, Georgia Institute of Technology & Emory University, Atlanta, GA 30332, USA

[2]Department of Biomedical Engineering, College of Engineering, Peking University, Beijing 100871, China

[3]School of Chemistry & Biochemistry, School of Chemical & Biomolecular Engineering, Georgia Institute of Technology, Atlanta, GA 30332, USA

*Author for correspondence: younan.xia@bme.gatech.edu

The application of nanostructured materials to solve biomedical problems has evolved into an active field of research known as nanomedicine. It is anticipated that nanomedicine will bring in many opportunities for more effective diagnosis and treatment of diseases, eventually causing paradigm shifts to the pharmaceutical and biotechnological industry [1–4]. In the context of cancer theranostics, therapeutic agents are increasingly integrated with nanostructures engineered with optimal size, shape and surface property to increase the solubility, prolong the blood circulation half-life, improve the pharmacokinetics and tumor targeting selectivity, and ultimately reduce the side effects. Specifically, nanostructures and their payloads have been favorably delivered into the tumor site by taking advantage of the pathophysiological conditions such as the enhanced permeability and retention (EPR) effect [5,6]. Targeting ligands, including organic molecules, peptides, antibodies and nucleic acids, have also been added onto the surfaces of nanostructures to target cancer cells through specific binding to the biomarkers overexpressed on their surfaces [5]. Additionally, it has been demonstrated that multiple types of theranostic agents can be delivered all together through the same carrier to enable combination therapy, with a potential to overcome some of the long-standing problems such as multiple-drug resistance and at the same time give real-time feedback on the treatment efficiency [7,8]. It is expected that precisely engineered nanomaterials will become the next-generation platform for cancer theranostics and other biomedical applications. In fact, a number of nanomedicine products have already been approved for clinical use and many others are under clinical trials [4,9].

As a unique class of nanostructured materials, Au nanocages have many attractive merits for a variety of biomedical applica-

Future Medicine part of fsg

tions [10–12]. Compared with solid Au nanoparticles, the hollow interiors and porous walls make Au nanocages ideal for controlled release and drug delivery as the drugs can be loaded in the interiors to increase the loading efficacy and help prevent the drugs from being released prior to use. In addition, Au nanocages are well-suited for cancer theranostics because: their size can be readily tuned in the range of 15–200 nm to optimize the biodistribution and tissue penetration; their atomically flat surface provides a well-defined substrate for quantitative functionalization and bioconjugation; the inert nature of Au provides Au nanocages with good biocompatibility and stability in the complicated *in vivo* environment; and their localized surface plasmon resonance (LSPR) peak can be precisely tuned to the near-infrared (NIR) region of 700–1200 nm to take advantage of the so-called 'transparent window' of soft tissues [12]. In the 'transparent window', light can penetrate deeply into soft tissues with very little attenuation, facilitating *in vivo* optical imaging and therapeutic applications [13,14]. For the conventional Au colloids with a solid interior and quasi-spherical shape, the LSPR peaks are typically limited to the visible region [15]. Only for Au nanostructures with anisotropic (e.g., rod, multipod and star) or hollow structures (e.g., shell, box and cage), can they display LSPR peaks in the NIR region.

A number of research groups have extensively explored the use of Au nanocages for a variety of biomedical applications. These include their use as contrast agents for optical coherence tomography, as vectors for drug delivery and tumor targeting, and as photothermal transducers for tumor destruction; some of these studies were covered in a review article published in *Nanomedicine (London)* in 2007 [16]. In recent years, the scope of applications for Au nanocages has been further expanded to include their use as optical probes for two- and three-photon luminescence imaging, as contrast agents for photoacoustic (PA) imaging, and as optical tracer for Cerenkov luminescence imaging. Radioactive isotopes have also been attached to their surfaces via post-synthesis modification, enabling their use as radioactive tracers for positron emission tomography (PET). In addition, new techniques for surface modification and drug encapsulation have been developed for targeted drug delivery, controlled release and cancer theranostics. The fate of Au nanocages upon uptake by cells or systemic administration into mice has also been studied. In this review article, we will start with a recap of the synthetic approach to Au nanocages, summarizing some of the latest progress in the large-scale production of Au nanocages and the synthesis of nanocages with sub-25 nm edge lengths. We then elaborate on the unique optical properties of Au nanocages, and highlight some recent advancements in optical imaging and cancer theranostics after the previous review in 2007 [16].

Synthesis & optical properties of Au nanocages

Gold nanocages can be readily prepared by taking advantage of the galvanic replacement reaction between a Au precursor, typically $HAuCl_4$ and a sacrificial template. This synthesis was first introduced by our group for the synthesis of Au nanocages with the use of multiply-twinned Ag nanoparticles as the template [17]. Afterward, the research has been largely focused on the use of single-crystal Ag nanocubes because of the easiness in controlling their uniformity in terms of both size and shape [17,18]. The reaction involved can be described as the following:

$$3Ag_{(s)} + AuCl_4^-{}_{(aq)} \rightarrow Au_{(s)} + 3Ag^+{}_{(aq)} + 4Cl^-{}_{(aq)}$$

Owing to a favorable difference in electrochemical potential between $AuCl_4^-$/Au (1.00 V) and Ag^+/Ag (0.80 V), the galvanic replacement reaction can occur spontaneously. It can be simply conducted by titrating $HAuCl_4$ into an aqueous suspension of Ag nanocubes under stirring and heating [17,18]. During the reaction, the Ag nanocubes underwent a series of morphological and structural changes as shown in Figure 1A. As detailed in a set of publications, the replacement reaction between a Ag nanocube and $HAuCl_4$ is initiated at a high-energy site on the surface and then continues toward the interior, generating a partially hollow nanostructure and then a nanobox [19]. Along with the dissolution of Ag template that empties the interior, an alloying process will simultaneously take place to facilitate the formation of Au–Ag alloy walls. After the formation of a nanobox, dealloying will start to occur, dissolving the Ag from the alloyed walls while generating pores and eventually lead to the formation of a Au-based nanocage [19,20].

During the titration, the main LSPR peak associated with the resulting nanostructures shifts to the red as the Ag nanocubes are transformed into nanoboxes and finally nanocages. By recording ultraviolet–visible–near infrared (UV–vis–NIR) spectra from the reaction solution, one can easily control the extent of the reaction and thus the porosity of the particles. Figure 1B shows the typical shift in LSPR peak position from visible to the NIR region during a titration process. Accordingly, colors of the samples gradually change from yellow to reddish brown, purple and blue (Figure 1C). The Au-based nanocages are typically composed of Au–Ag alloys, with the Au content varying from 40 to 60% by weight. In meeting the requirements of some biomedical applications, the remaining Ag can be selectively removed using etchants based on

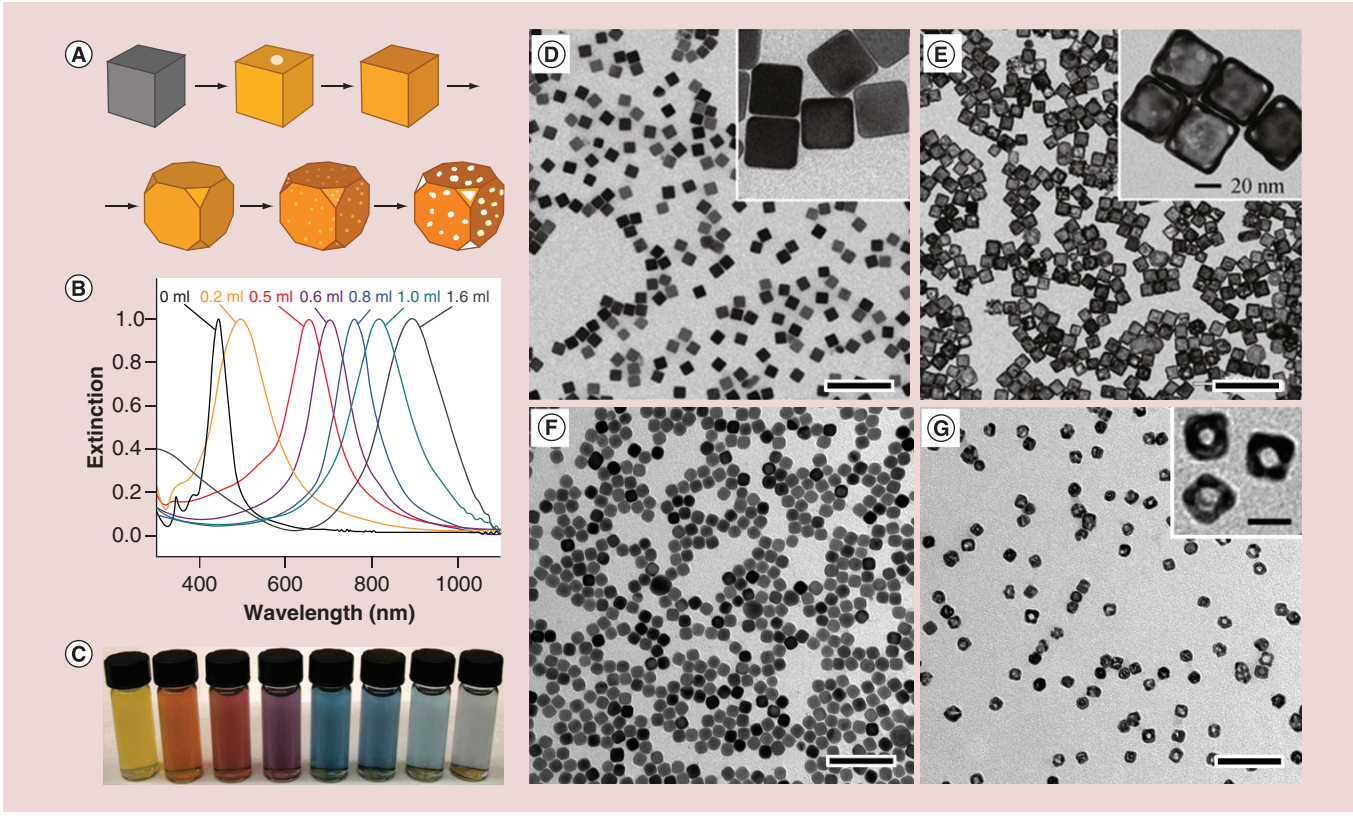

Figure 1. Synthesis and characterization of Au nanocages. **(A)** Schematic illustration showing the structural evolution at different stages of a synthesis; **(B)** UV–vis spectra of samples obtained after titration of different amounts of $HAuCl_4$ into a suspension of Ag nanocubes; **(C)** photograph of the corresponding samples in **(B)**, showing the color changes [20]; **(D–G)** TEM images of Ag nanocubes with edge lengths of **(D)** 40 nm [11] and **(F)** 18 nm [34], respectively, along with their corresponding Au nanocages. The scale bars are 250 nm in **(D & E)**, 100 nm in **(F & G)** and 20 nm for the insets.
Reproduced with permission from [11,20,34].

$Fe(NO_3)_3$, NH_4OH or H_2O_2, without destructing the hollow and porous structure [21,22].

In addition to their precisely tunable LSPR peak positions, Au nanocages generally possess optical cross-sections that are 5–6 orders of magnitude higher than those of molecular dyes [23]. To quantitatively compare Au nanocages with other types of Au nanostructures, an optofluidic device was developed to measure their optical cross-sections and photothermal conversion efficiency [24]. In comparison with Au nanorods and nanohexapods, Au nanocages with LSPR peak at the same position (*ca.* 800 nm) were found to have the largest absorption cross-section (σ_a) of 12.4 ± 1.2 × 10^{-15} m^2, which is in agreement with theoretical calculations. In comparison, the σ_a of Au nanorods or nanohexapods was less than half of that of the nanocages. The total extinction cross-sections (σ_e) of Au nanocages could also be derived by UV–vis–NIR spectroscopy or theoretical calculation, while the σ_a could be derived by PA microscopy or theoretical calculation [25,26]. In the case of Au nanocages with an edge length of 32 nm and a wall thickness of 4 nm, σ_a was found to be approximately 95% of σ_e, making them strong candidates for photothermal applications [25].

An obvious challenge that can limit the application of nanomaterials in medicine is the ability to synthesize nanoparticles in large quantities, together with good uniformity in terms of size and shape. For Au nanocages, the bottleneck lies in the scale-up synthesis of Ag nanocubes that are used as sacrificial templates for the galvanic replacement reaction. Our group pioneered the synthesis of Ag nanocubes through the polyol method that reduces a silver nitrate ($AgNO_3$) precursor with ethylene glycol (EG) in the presence of poly(vinyl pyrrolidone) (PVP) [18]. In this approach, EG is typically heated to 140–160°C under ambient atmosphere to generate glycolaldehyde [27], whose aldehyde group can reduce Ag^+ ions to Ag atoms, initiating the nucleation and growth of Ag nanocrystals. A trace amount of Cl^- (on the ppm level), coupled with the oxygen from air, can selectively dissolve the defective twin seeds while leaving the single-crystal counterparts unaffected [28]. Meanwhile, PVP can serve as a capping agent that promotes the formation of Ag{100} facets, resulting in the formation of well-defined nan-

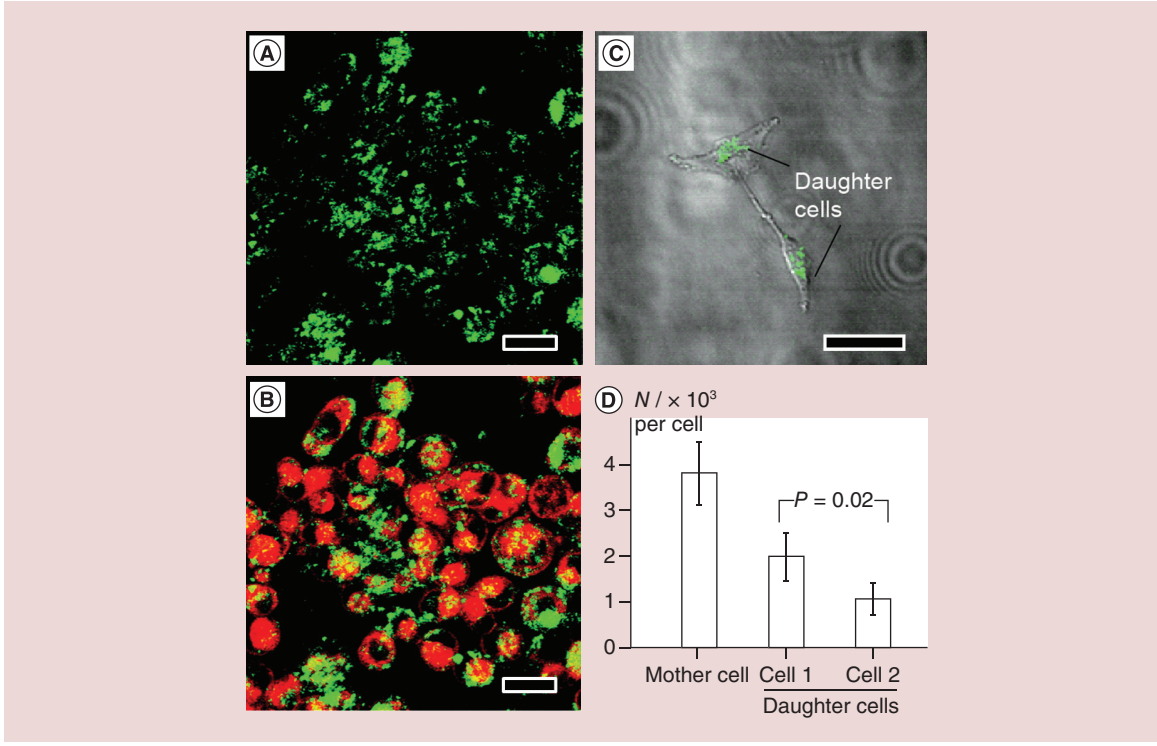

Figure 2. Two-photon luminescence imaging of cells *in vitro* with the use of Au nanocages as contrast agents.
(A) Confocal microscopy image of EGFR-overexpressing U87-MG cells, after incubation with FM4-64 dye and Au nanocages, showing the luminescence from Au nanocages only; **(B)** superimpositions of the luminescence from Au nanocages and red fluorescence from FM4-64 [36]; **(C)** confocal microscopy image of two daughter cells divided from a month cell containing Au nanocages; and **(D)** quantitative data showing the distributions of Au nanocages during cell proliferation. The daughter cells did not share the Au nanocages equally during cell division [38]. The scale bars are 20 μm for **(A & B)** and 50 μm for **(C)**.
Reproduced with permission from [36,38].

ocubes [29]. In recent years, the synthesis was further refined by introducing S^{2-} or HS^- into the system, and by substituting $AgNO_3$ with silver trifluoroacetate (CF_3COOAg) to improve the yield, size distribution and reproducibility. With S^{2-} or HS^- in the reaction system, Ag_2S nanocrystallites, formed upon the injection of Ag^+ precursor, can serve as nuclei to generate single-crystal Ag seeds [30,31]. Using CF_3COOAg as a precursor helps to eliminate the NO_2 generated from the decomposition of the nitrate group from $AgNO_3$, avoiding its unwanted effects on the nucleation and etching processes [32]. Using a modified protocol, uniform Ag nanocubes can be produced on a scale of approximately 1 g per batch with edge lengths ranging from 30 to 70 nm (Figure 1D). Each gram of Ag nanocubes can be converted into approximately 0.7 g of Au nanocages by titration with $HAuCl_4$ (Figure 1E) [27,33].

The size of nanoparticles can greatly affect their *in vivo* biodistribution profile and intratumoral distribution, which are critical to biomedical applications. To meet the requirement of a broad size range for various applications, seed-mediated growth was adapted for the synthesis of Ag nanocubes with edge lengths ranging from 18 to 200 nm. In this case, single-crystal Ag seeds with a size of 30–40 nm were first prepared using the method described above. After washing with acetone, the seeds were resuspended into EG and subjected to further growth in the presence of $AgNO_3$ and PVP at 150°C. The sizes of the Ag nanocubes were determined by the ratio of $AgNO_3$ to the seeds. To prepare small Ag nanocubes with an edge length down to 18 nm, the polyol synthesis was modified by replacing the EG with diethylene glycol. Owning to a higher viscosity than EG, diethylene glyco was found to facilitate the formation of small single-crystal Ag nanocubes with an edge length of 18–32 nm by slowing down the reaction rate (Figure 1F) [34]. Based on these Ag nanocubes, Au nanocages with an edge length as short as 20 nm were obtained (Figure 1G). Most recently, Ag nanocubes as small as 13 nm in edge length were successfully prepared [35], which could be used to produce Au nanocages with a size approaching 15 nm.

Optical imaging

Owing to their tunable LSPR peaks and large σ_a, Au nanocages are great tracers or contrast agents for a num-

ber of optical imaging modalities [26]. To these ends, Au nanocages have been explored for two- and three-photon luminescence imaging [36–39], as well as PA and optical coherence tomography imaging [40–42]. In addition, Au nanocages have been applied to a novel imaging modality based on Cerenkov luminescence [43].

Two-photon & three-photon luminescence imaging

For Au nanostructures such as nanocages or nanorods, they can be excited *via* a two-photon absorption mechanism to emit relatively strong luminescence [36,44]. In this case, an electron on the ground state will absorb two photons simultaneously and be excited to the *s-p* conduction band. When the excited electron recombines with a hole in the *d*-band, a photon with an energy twice that of the incident light will be emitted [45–47]. When the wavelength of the excitation laser overlaps with the LSPR peak of the Au nanostructures, the luminescence will be greatly enhanced because of marked increase in excitation efficiency [36]. As a result, two-photon luminescence imaging can be readily applied to quantify the uptake of Au nanostructures by living cells. For example, with the use of antibody-conjugated Au nanocages, U87-MG glioblastoma cells overexpressing EGF receptor (EGFR) were observed to emit strong luminescence under the excitation by a laser of 760 nm in wavelength (Figure 2A & B). The data derived from the luminescence intensities were consistent with those obtained from inductively coupled plasma MS analysis, indicating a good quantitative property with this method [36]. In a similar approach, the fate of Au nanocages in U87-MG glioblastoma cells during cell proliferation was also quantitatively assessed with cyclic Arg-Gly-Asp-D-Tyr-Lys, or c(RGDyK), functionalized Au nanocages [37]. It was found that the Au nanocages were not equally shared between the two daughter cells, and a small portion of Au nanocages was released into the culture medium during cell division (Figure 2C & D) [38]. However, the detailed mechanism of excretion of Au nanocages from the cells remain to be resolved.

With the wavelength of excitation laser being positioned in the 'transparent window' of soft tissues, two-photon microcopy is well-suited for *in vivo* tracking and quantitative assessment of Au nanocages. To this end, two-photon microscopy was combined with Au nanocages for labeling and tracking of human mesenchymal stem cells (hMSCs) [39]. In this study, the

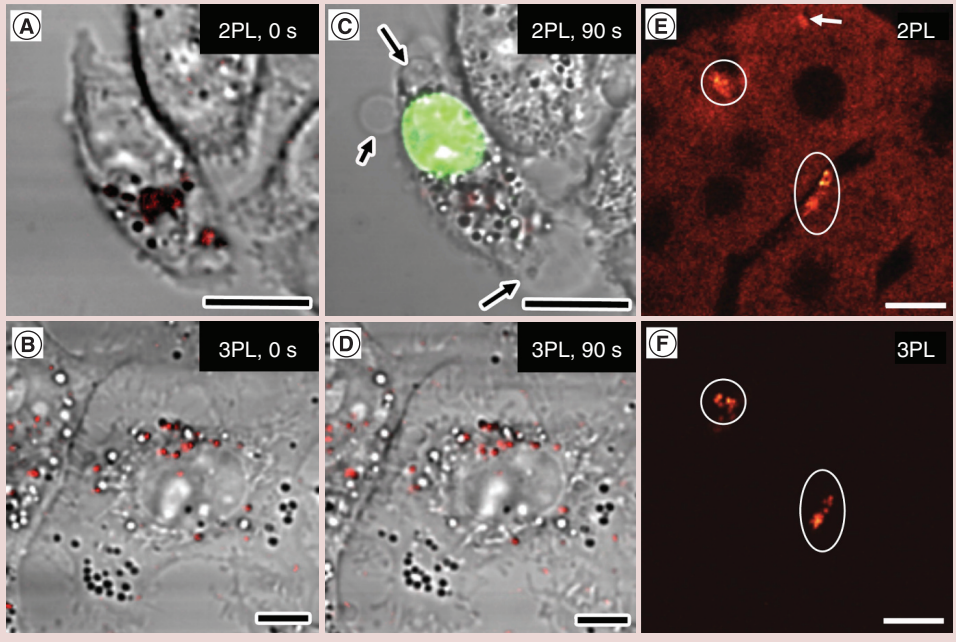

Figure 3. Comparison of two-photon and three-photon luminescence imaging. **(A)** Two-photon luminescence image and **(B)** three-photon luminescence image of Au nanocages (red color) in KB cells right after laser scanning. **(C)** Two-photon luminescence image of the same cell as in **(A)** after scanning with 760 nm laser at 1.9 mW for 90 s. Membrane blabbing (arrowed) was observed as indicated by ethidium bromide staining (green color). **(D)** Three-photon luminescence image of the same cell as in **(B)** after scanning with 1290 nm femtosecond laser at 4.0 mW for 90 s. **(E)** Two-photon and **(F)** three-photon luminescence image of Au nanocages (white circles) in the same liver tissue. In two-photon luminescence imaging normal tissue give strong autofluorescence (arrowed) [37]. Scale bars in all images are 10 μm.
Reproduced with permission from [37].

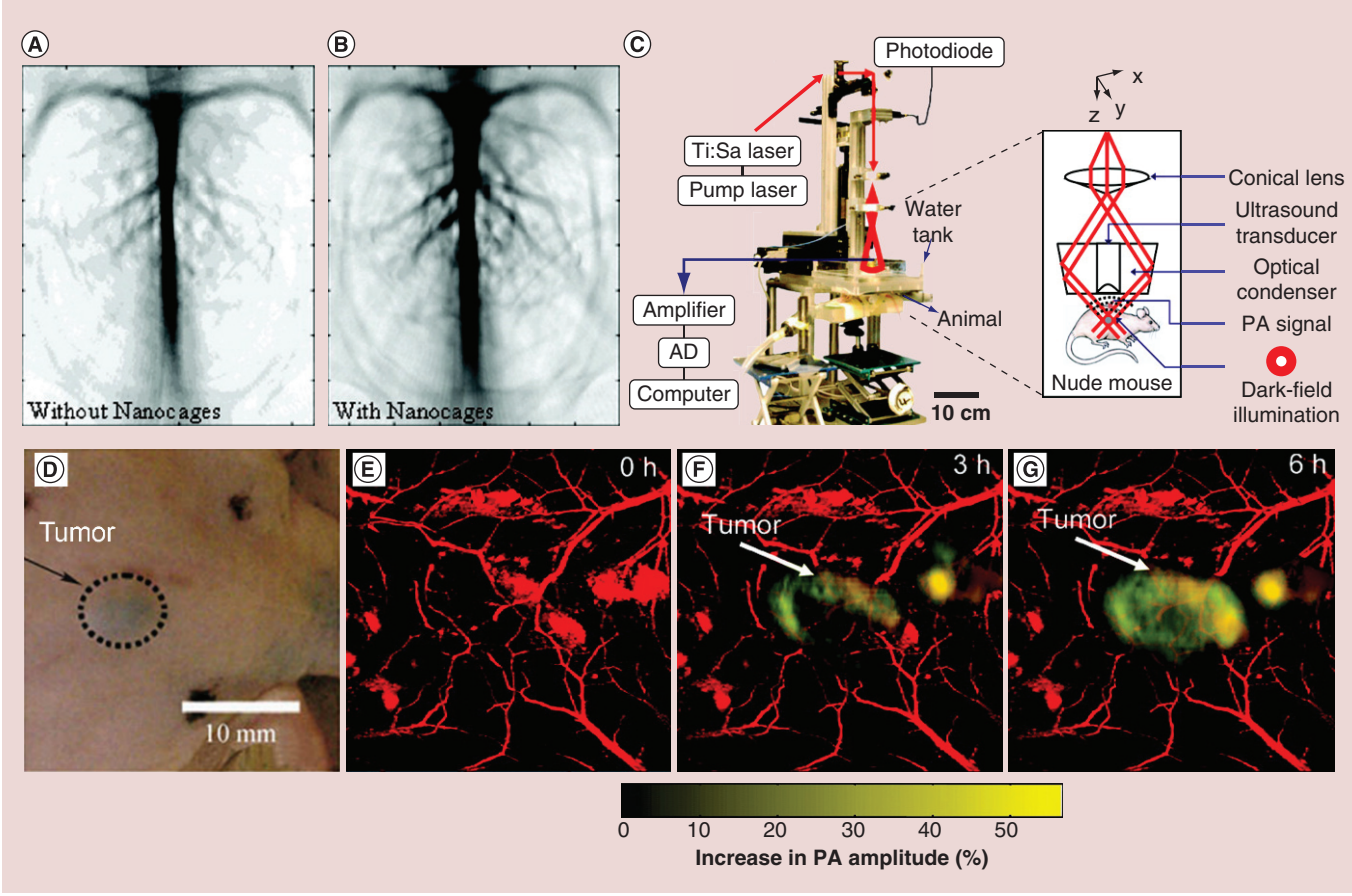

Figure 4. Photoacoustic tomography imaging using Au nanocages as contrast agent. **(A)** Photoacoustic tomography (PAT) imaging of rat cerebral cortex without contrast agent; **(B)** Contrast enhancement of PAT imaging of rat cerebral cortex with 50 nm Au nanocages as contrast agent. Picture took after 2 h of the final injection [40]. **(C)** The schematic and photograph of the PA microscope used for *in vivo* molecular PAT imaging of melanomas, with [Nle^4, D-Phe^7]-α-MSH-Au nanocages as contrast agents. **(D)** Photograph of nude mice with B16 melanomas xeongraft. **(E–G)** Time-lapse PA images of the B16 melanomas after tail vein injection with 100 μl of 10 nM of [Nle^4, D-Phe^7]-α-MSH-Au nanocages. The background vasculature images (red) were acquired using the PA microscope at 570 nm (ultrasonic frequency = 50 MHz), and the melanoma images (gold) were acquired using the PA microscope at 778 nm (ultrasonic frequency = 10 MHz) [42].
Reproduced with permission from [40,42].

hMSCs labeled with Au nanocages could be readily located, which migrated to and homed at the glioblastoma regions after tail vein injection in nude mice. The labeling of hMSCs was achieved by direct incubation of the cells with the as-prepared 45 nm Au nanocages. Images for quantitative analysis were captured using two-photon microscopy at 1 week post injection. The Au nanocages did not appear to compromise the function of hMSCs and could remain in the cells for at least 4 weeks, enabling potential long-term monitoring of cell migration [39]. When combined with the latest targeting methods, Au nanocages hold great potential for *in vivo* tracking of cancer cells to offer insights into the metastasis of cancer.

When the LSPR peak of Au nanocages overlaps with the wavelength of excitation laser, the energy from absorbed photon will largely be converted to heat rather than luminescence. The heat may adversely impact biological samples [37]. To address this issue, the use of Au nanocages was subsequently explored for three-photon luminescence. When excited by a femtosecond laser at 1290 nm, the Au nanocages emitted a broad three-photon luminescence that was one order of magnitude stronger than that from a control sample such as Au nanospheres or Ag nanocubes [37]. In an effort to evaluate the photothermal toxicity, two groups of KB cells (a carcinoma cell line) containing similar number of Au nanocages were illuminated by a 760 nm laser for two-photon imaging and a 1290 nm laser for three-photon imaging, respectively, as shown in Figure 3A & B. After 90 s of imaging with the 760 nm laser at 1.9 mW, cell membrane blebbing (arrowed) was observed. The membrane integrity was also confirmed to be compromised by ethidium bromide labeling (Figure 3C).

In contrast, no damage to the plasma membrane occurred after imaging for 90 s with a 1290 nm laser at 4.0 mW (Figure 3D). Another advantage for three-photon luminescence imaging is that the excitation at 1290 nm matches the 'second transparent window' of 1000–1350 nm, in which the autofluorescence from soft tissues can be completely suppressed [37]. As clearly demonstrated in Figure 3E & F, the two-photon luminescence image displays a much stronger background than the three-photon luminescence image, primarily due to the autofluorescence from the liver tissue.

Photoacoustic microscopy & photoacoustic tomography

As two newly developed biomedical imaging modalities, photoacoustic microscopy (PAM) and photoacoustic tomography (PAT) offer noninvasive and volumetric imaging of scattering media with deep penetration and high spatial resolution [41,48–50]. When a pulsed or chopped laser is delivered to tissue, some of the energy will be absorbed and converted to heat. The rapid heating will cause the tissue to expand. However, the tissue will contract as soon as the laser is in the off state. The expansion and contraction will generate acoustic signals that can be detected by ultrasonic transducers and converted into an image [49]. To this end, Au nanocages can greatly enhance the contrast of PA imaging due to their strong photothermal capability [49].

In one collaboration, our group and the Wang group extensively explored the use of Au nanocages as a new class of contrast agents for PA imaging. For example, when Au nanocages coated with PEG (MW ≈ 5000) circulated through the vasculature in rat cerebral cortex, there was an substantial enhancement in PA signals (Figure 4A & B). The enhancement for the optical absorption by blood could reach a level of 81% within 2 h after the final injection [40]. The *ex vivo* imaging study of Au nanocages in sentinel lymph nodes also suggested a great enhancement with deep penetration, when compared with the conventional methods for sentinel lymph node mapping [41]. In another study, *in vivo* PA imaging of melanomas was achieved by using Au nanocages conjugated with [Nle^4, D-Phe^7]-α-melanocyte stimulating hormone ([Nle^4, D-Phe^7]-α-MSH-Au nanocages) as contrast agents. The [Nle^4, D-Phe^7]-α-MSH-Au nanocages displayed active tumor targeting with high sensitivity and specificity [42]. Figure 4C shows a typical experimental setup of the PA imaging system. Figure 4D–G, shows the photograph and time lapse PAM images of subcutaneous melanoma in a nude mouse. At 6 h post injection, the average PA signal intensity increased by 36%, indicating accumulation of Au nanocages in the targeted sites. It is worth noting that the [Nle^4, D-Phe^7]-α-MSH-Au nanocages achieved an increased tumor uptake of approximately 300% higher than the nontargeted Au nanocages (the control), demonstrating that Au nanocages can be delivered into a tumor with higher selectivity through active targeting.

Cerenkov luminescence imaging

The optical imaging modalities listed above all utilize the intrinsic optical properties arising from the collective oscillation of conduction electrons in Au nanocages (or other types of Au nanostructures). By incorporating a radioactive isotope into the lattice of Au nanostructures, it is also feasible to create new optical properties for imaging applications. One of such properties is Cerenkov luminescence, which refers to the electromagnetic radiation emitted by a charged particle passing through a dielectric medium at a speed greater than the speed of light in that medium. Particles originating from the radioactive decay of a radionuclide could easily fulfill the requirement and thus generate Cerenkov luminescence.

In one study, a controlled amount of radioactive ^{198}Au was directly incorporated into the lattice of Au nanocages by replacing some of the $H^{197}AuCl_4$ precursor with $H^{198}AuCl_4$ during the galvanic replacement reaction with Ag nanocubes (Figure 5A). The radioactivity of the Au nanocages could be precisely controlled by varying the proportion of $H^{198}AuCl_4$ precursor [43]. Nontargeted, PEGylated ^{198}Au-doped Au nanocages with an average edge length of 33 nm has been synthesized and then applied to Cerenkov luminescence imaging with a mouse EMT-6 tumor model. As shown in Figure 5B, the ^{198}Au-doped Au nanocages exhibited targeted accumulation in the tumor based on the EPR effect at 24 h post injection. The direct incorporation of ^{198}Au atoms into the crystal lattice of Au nanocages allowed us to accurately analyze the biodistribution of nanoparticles, without worrying about the chemical stability of the linker and chelator.

Positron emission tomography

Nuclear imaging modalities such as PET and single photon emission computed tomography (SPECT) have been widely used in clinics for the diagnostics of cancer and cardiovascular diseases [51,52]. With the use of proper radioactive isotopes, these tools can be employed to accomplish noninvasive, whole-body imaging with high sensitivity and deep imaging depth.

To better understand the pharmacokinetics and biodistribution profiles of Au nanocages, PET imaging was utilized to visualize and monitor their *in vivo* behavior. After labeling their surface with $^{64}Cu^{2+}$ through a chelating agent, the pharmacokinetics and biodistribution profiles of both 30- and 55 nm Au nanocages were

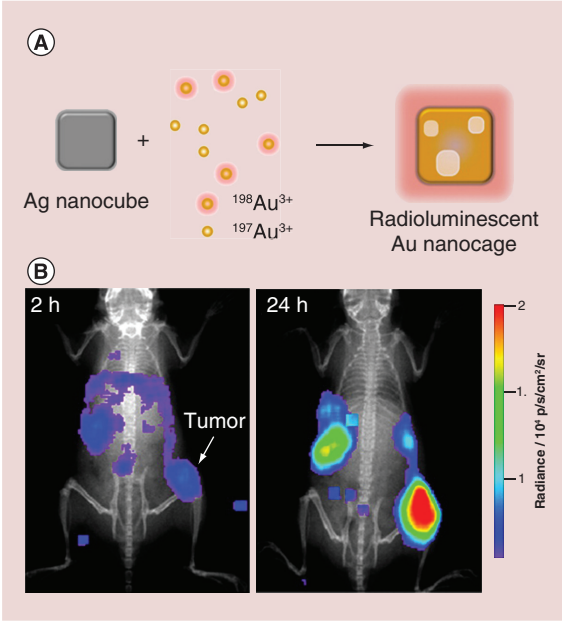

Figure 5. Direct incorporation of ^{198}Au into the crystal lattice of Au nanocages for Cerenkov luminescence imaging. (A) Schematic illustration showing the incorporation of ^{198}Au into Au nanocages; **(B)** Cerenkov luminescence images recorded 2 and 24 h post tail vein injection of 30 nm PEGylated ^{198}Au-doped Au nanocages, showing their capability of tumor targeting [43].
Reproduced with permission from [43].

studied with EMT-6 tumor bearing mice [53]. In this study, the surface of Au nanocages were functionalized with a widely used chelator, 1,4,7,10-tetraazacyclododecane-1,4,7,10-tetraacetic acid (DOTA), by reacting with polyethylene glycol thiol (NH_2-PEG-SH, MW ≈ 5000) and then DOTA-mono(*N*-hydroxysuccinimide ester) (DOTA-NHS-ester). The $^{64}Cu^{2+}$ ions were chelated to the DOTA group, followed by purification with centrifugation, and testified by fast protein liquid chromatography (Figure 6A). After 24 h, both the small and large ^{64}Cu-labeled Au nanocages (^{64}Cu-DOTA-PEG-Au nanocages) showed increased uptakes in the tumor. Compared with the 55 nm counterpart, the 30 nm Au nanocages exhibited improvement in both pharmacokinetics and blood circulation, together with decreased uptakes by liver and spleen [53]. Meanwhile, the 30 nm Au nanocages were also found to be able to penetrate into the central region of the tumor (Figure 6B & C). This study indicates that by tuning the size of nanoparticles it is possible for researcher to design the Au nanocage-based nanomedicine with desirable biodistribution and intratumoral distribution profiles.

Therapeutic applications

Photothermal cancer treatment

In addition to diagnosis, the strong photothermal effect of Au nanocages can also be used to directly

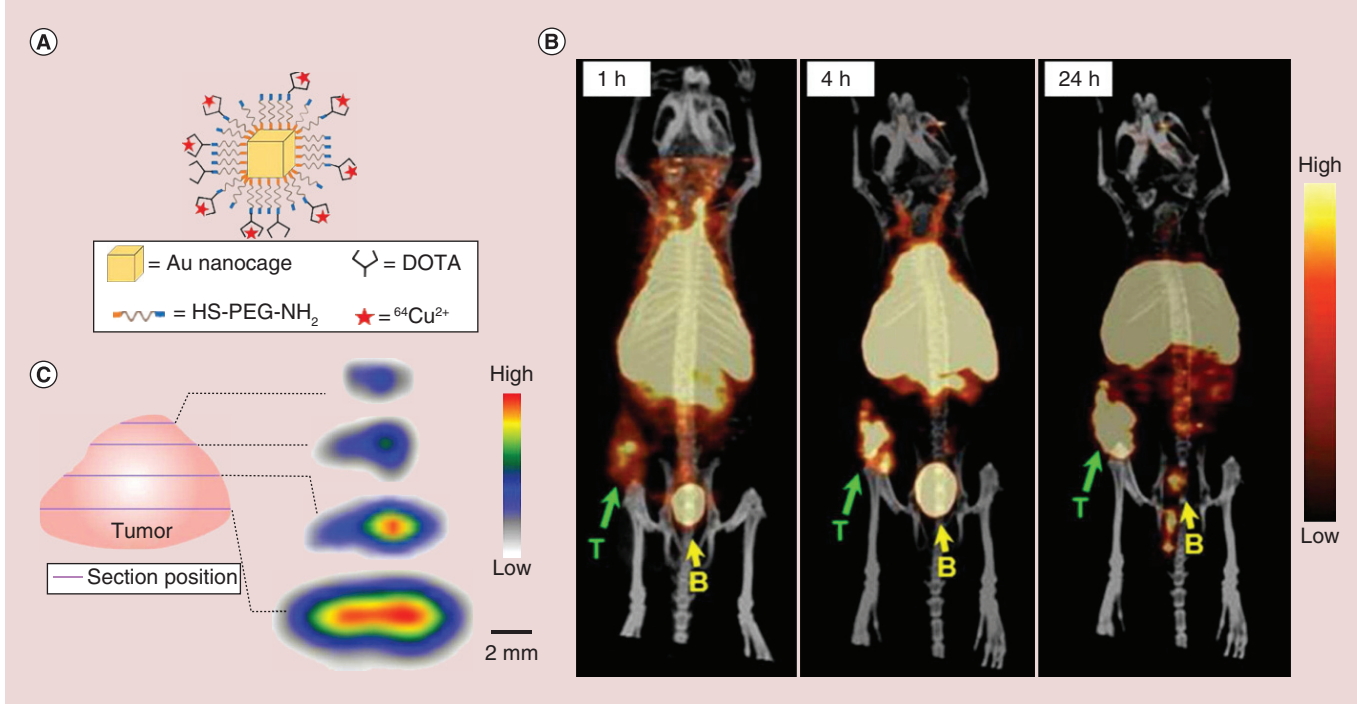

Figure 6. PET/CT imaging of ^{64}Cu-DOTA-PEG-Au nanocages in an EMT-6 tumor mouse model. (A) Schematic illustration of the surface-modified Au nanocages; **(B)** PET/CT images of 30 nm ^{64}Cu-DOTA-PEG-AuNCs in a mouse bearing an EMT-6 tumor at 1, 4 and 24 h post injection (3.7 MBq injection per mouse). T: tumor; B: bladder. **(C)** PET/CT images recorded from different cross-sections of an EMT-6 tumor, showing the intratumoral distribution of Au nanocages [53].
Reproduced with permission from [53].

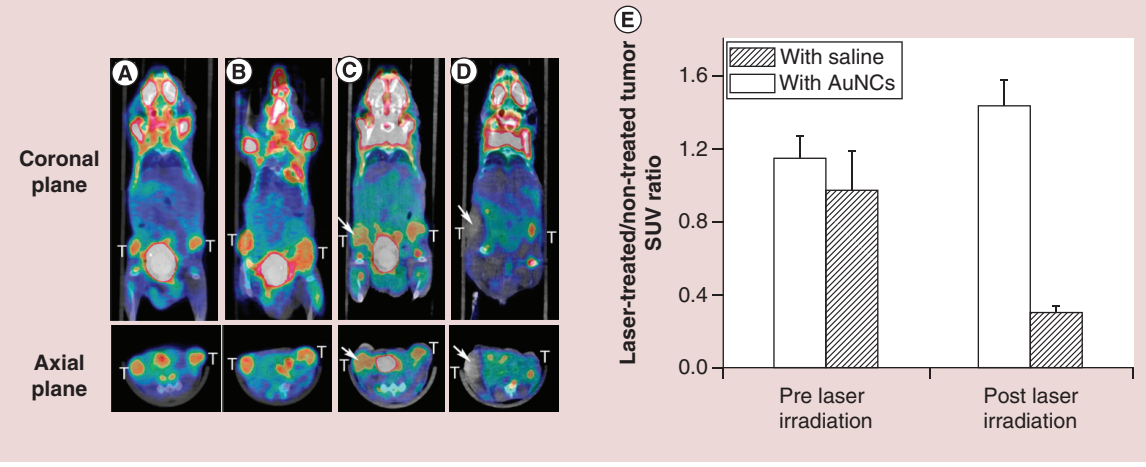

Figure 7. Photothermal cancer treatment with Au nanocages. ^{18}F-FDG PET/CT images recorded from mice bearing breast cancer. Either saline or suspension of Au nanocages, was intravenously administrated before laser treatment. **(A–D)** show a saline-injected mouse **(A)** prior to and **(C)** after laser irradiation; A Au nanocages-injected mouse **(B)** prior to and **(D)** after laser irradiation. The white arrows indicated the tumors that were exposed to the diode laser at a power density of 0.7 W cm^{-2} for 10 min. (e) A plot showing the metabolic changes of laser-treated tumor to nontreated tumor from ^{18}F-FDG standardized uptake values (SUV, $p < 0.001$) [61]. Reproduced with permission from [61].

treat cancer or to trigger and control the release of a drug. In this case, the generated heat is used to selectively destruct cancer cells during or post diagnostics. To facilitate *in vivo* applications, photothermal transducers with strong absorption in the NIR region were needed [54–58]. *In vitro* studies indicate that Au nanocages have higher photothermal conversion efficiency than Au nanohexapods and nanorods of roughly the same dimension, while maintaining good photothermal stability and low cell toxicity [59]. In comparison with conventional organic dyes, Au nanocages possess precisely tunable LSPR peaks in the NIR region, as well as considerably larger σ_a, making them an ideal candidate for photothermal therapy [60].

In an initial study, Au nanocages were conjugated with anti-EGFR for *in vitro* studies with SK-BR-3 breast cancer cells [58]. The Au nanocages were proven to be effective photothermal transducers for site-specific destruction of cancer cells. Following this work, Au nanocages were further explored for *in vivo* photothermal treatment in a bilateral tumor model [61]. In this study, each tumor-bearing mouse was intravenously injected 100 µl 10 mg/ml of nontargeted, PEGylated Au nanocages with an average edge length of 48 nm. At 72 h post injection, photothermal treatment was conducted by exposing the tumor to an 808 nm diode laser at a power density of 0.7 W/cm^2 for 10 min. The region of interest was rapidly heated up to 50°C within 1 min, and reached 55°C at 2 min. To evaluate the efficacy of the treatment, PET imaging of ^{18}F-fluorodeoxyglucose (^{18}F-FDG) was conducted to monitor the change to metabolic activity in the tumor before and after the treatment (Figure 7A–D). Without laser irradiation, both the mice injected with saline and Au nanocages exhibited high levels of ^{18}F-FDG uptake by the tumors with no significant difference (Figure 7E). The PET imaging reveals that the tumor uptake of ^{18}F-FDG for the Au nanocages-injected mouse was significantly reduced at 24 h post irradiation, indicating decreased metabolic activity caused by photothermal therapy (Figure 7C & D). The normalized data show a drastic decrease of 70% in tumor metabolic activity after the treatment, while no significant change was observed for the saline-injected control group (Figure 7E).

Controlled release

The surface of nanoparticles often needs modification in order to achieve optimal circulation and delivery *in vivo* [62]. Among them, PEGylation is most widely used to provide nanoparticles with a 'stealth' property to prevent them from rapid clearance by mononuclear phagocyte system [63]. Furthermore, the PEGylated nanoparticles can serve as a new platform for further surface modification. To this end, a quantitative understanding of the coverage density of PEG chains on the surface of nanoparticle is of significant importance for reproducible surface modification. Four different methods were utilized for quantifying the coverage density of PEG chains on Au nanostructures [64]. The first two methods used conventional amine assays to measure the concentration of unreacted HS-PEG-NH_2 molecules in the supernatant after incubation with Au nanostructures. The other two methods deter-

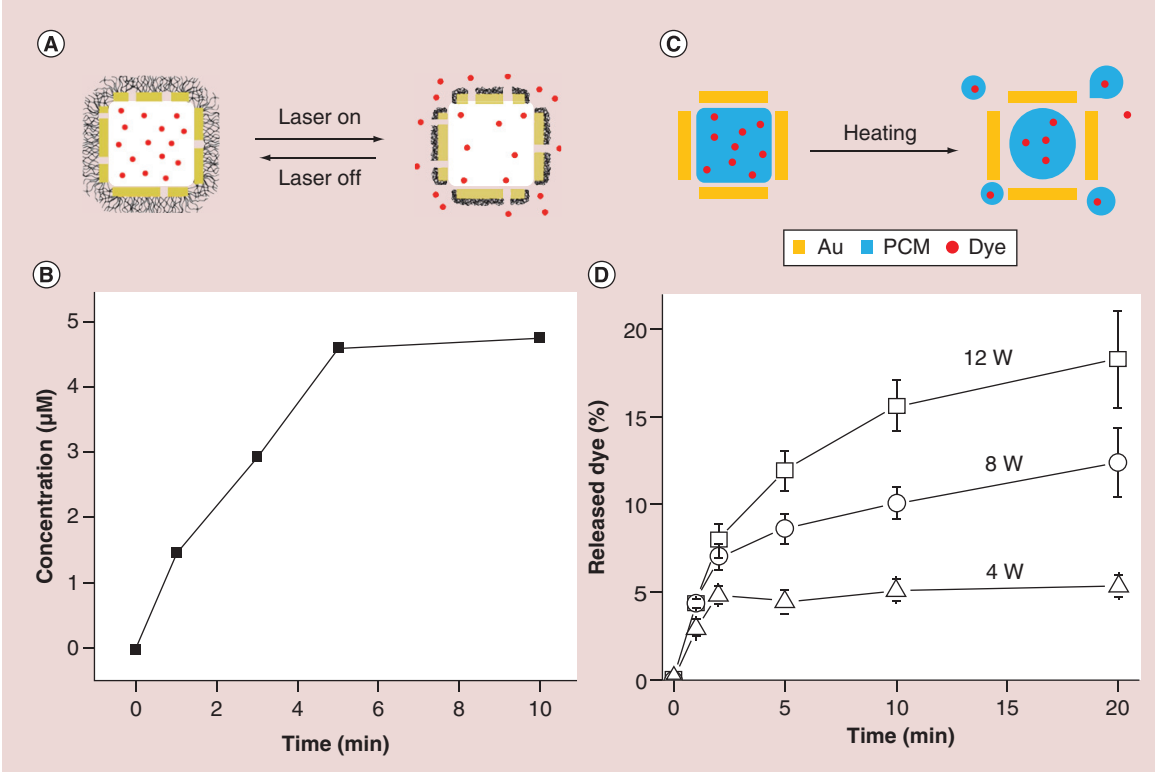

Figure 8. Gold nanocages as delivery vehicles for controlled drug release. (A) A schematic illustration of controlled release enabled by a smart polymer, poly(*N*-isopropylacrylamide), coated on the surface of Au nanocages; **(B)** release profile of Dox from the system shown in **(A)**, as triggered by a NIR laser [67]; **(C)** a schematic illustration of controlled release assisted by a phase-change materials (PCMs); and **(D)** release profiles of the dye from PCM-containing Au nanocages shown in **(C)** when exposed to HIFU [68].
Reproduced with permission from [67,68].

mined the 'active' amino groups on the surface of a Au nanostructure through coupling between the terminal amino groups of adsorbed -S-PEG-NH_2 chains and fluorescein isothicyanate (FITC) or a chelator for Cu^{2+} ion. [64]. After quantifying the coverage density of PEG, it was found that the number of -S-PEG-NH_2 chains per Au nanocage decreased in the order of: -S-PEG_{3000}-NH_2 > -S-PEG_{5000}-NH_2 >> -S-$PEG_{20,000}$-NH_2. The adsorption kinetics of the HS-PEG-NH_2 molecules was further investigated. In general, the adsorption of HS-PEG-NH_2 could reach equilibrium within 150 min for all the Au nanostructures tested. However, it was found that the adsorption of -S-PEG-NH_2 chains onto Au nanorods covered by cetyltrimethylammonium bromide was much slower than that of PVP-capped Au nanocages and the citrate-caped Au nanoparticles.

Surface modification also enabled the detection of protease activity by taking advantage of the fluorescence quenching properties of Au nanoparticles. This concept was demonstrated by conjugating FITC to the surface of a Au nanocage through the use of a protease-sensitive linker -GKGPLGVRGC-NH_2 [65]. Once attached to the surface of a Au nanocage, the fluorescence signal from FITC was quenched because of the nano-surface energy transfer effect [66]. In the presence of matrix metalloproteases, however, FITC was selectively released due to enzyme cleavage and the fluorescence would be recovered. The fluorescence intensity was linearly proportional to the incubation time in the period from 10 to 120 min and began to level off after 6 h. This approach is of potential use for controlled drug release in response to the concentration of matrix metalloproteases.

The unique hollow structure of Au nanocages allows us to load them with a large amount of drug, making them viable as drug delivery vehicles. To date, molecules such as enzymes, dyes, anticancer drugs and phase change materials (PCMs) have all been encapsulated and then released with an external trigger [67,68]. In an early study, the surface of Au nanocages was conjugated with a thermally responsive smart polymer for the controlled release of a preloaded drug in response to temperature rise caused by localized heating [67]. As shown in Figure 8A, the smart polymer, poly(*N*-isopropylacrylamide), whose conformation can be changed

in response to temperature variations, was directly grafted to the surface of Au nanocages using the Au–S coupling chemistry. The temperature above which the payloads will be released is determined by the low critical solution temperature (LCST) of the smart polymer, which can be tuned by incorporating acrylamide into the polymer side chain [69]. The polymer chains exist in a stretched conformation at a temperature below the LCST, sealing the pores on the Au nanocages. Upon heating to a temperature above the LCST, the polymer chains collapse and expose the pores on the nanocages, causing the drug to release from the interiors of the nanocages. Figure 8B shows a release profile of doxorubicin (Dox) from the Au nanocages at 45°C [67]. The therapeutic effect of the released drug was also assessed *in vitro* with breast cancer cells. Under the irradiation of a pulsed laser at a power density of 20 mW cm^{-2} for 2 and 5 min, Dox was effectively released to kill the cancer cells. The heating could also be accomplished with high-intensity focused ultrasound (HIFU) to manage the drug release profile with deeper penetration than an NIR laser system [70].

Recently, another theranostic system was demonstrated with a combination of both a contrast agent for PA imaging and a controlled drug release mechanism by HIFU [68]. Instead of pure therapeutic drugs, the hollow interiors of Au nanocages were filled with drug-doped PCM whose melting point was carefully tuned to 38–39°C [68,71]. Once the drug was dissolved in the PCM, the mixture could be loaded into the cavities of Au nanocages through simple incubation. Aside from assisting in drug loading, PCMs also serves as a 'gate keeper' to control the drug release in response to temperature increase [68]. As shown in Figure 8C, since PCM has a sharp transition in its physical states between solid and liquid, it can hold up the payload inside the Au nanocages below its melting point. Once the temperature is increased beyond the melting point (e.g., due to exposure to HIFU), the payloads will be released by together the melted PCM. As shown in Figure 8D, the release profile can be controlled by either manipulating the power of HIFU or the duration of exposure.

Conclusion & future perspective

Gold nanocages have a unique combination of physicochemical properties stemming from the chemistry of Au, the electronic structure of nano-sized Au, as well as the hollow interiors and porous walls. These properties can be tailored to fit the needs of multiple theranostic applications. Significant progress has been made in scaling-up the production of Au nanocages, as well as in the synthesis of Au nanocages with sizes as small as 15 nm, allowing them to be used for an array of biomedical applications. Specifically, their tunable LSPR peaks have enabled their use as optical tracers or contrast agents for *in vitro* and *in vivo* PA imaging. Following PA tomography, the Au nanocages can serve as transducers to kill cancer cells through the photothermal effect thanks to extraordinarily large absorption cross-sections. When labeled with radioactive isotopes, Au nanocages can also be turned into tracers for cancer diagnostics *in vivo* by PET imaging. In addition, the hollow interiors and porous walls of Au nanocages make them perfect carriers for the loading and release of drugs in a controlled manner. In collaborating with a number of groups, we have developed a more profound understanding of the synthesis, properties and biomedical applications of Au nanocages. Most of the recent developments are briefly summarized in this review article. Like other types of nanoparticles, the translational use of Au nanocages will be largely determined by their biodistribution and pharmacokinetics *in vivo*. By engineering their size and controlling their surface chemistry, it will be feasible to achieve favorable biodistribution profiles for Au nanocages, with minimal nonspecific accumulation in healthy tissues and reduced clearance by microphysiological systems. For the clearance of Au nanocages from the body, one possible solution is to break them into small pieces after theranostics. Because of their hollow interiors and porous, ultrathin walls, it is more promising to achieve this goal for Au nanocages as compared with their solid counterparts. At the moment, the greatest challenge is to develop a robust synthesis of Au nanocages with walls below 1 nm and demonstrate the associated techniques to fragment them *in vivo* into small pieces less than 5 nm in size. After reading through this brief introduction to the most recent developments, we hope the readers will have a better understanding of the great potential of Au nanocages and will find the motivation to develop new biomedical applications for this novel class of nanomaterials.

Financial & competing interests disclosure

This work was supported in part by a research grant from the National Cancer Institute (1R01 CA 138527), an NIH Director's Pioneer Award (DP1 OD000798) and startup funds from the Georgia Institute of Technology. As a visiting PhD student from Peking University, B.P. was also partially supported by the China Scholarship Council. The authors have no other relevant affiliations or financial involvement with any organization or entity with a financial interest in or financial conflict with the subject matter or materials discussed in the manuscript apart from those disclosed.

No writing assistance was utilized in the production of this manuscript.

Executive summary

Synthesis & optical properties of Au nanocages

- Gold nanocages can be conveniently prepared, with good uniformity and in large quantity (>0.7 g/batch), through the galvanic replacement reaction between Ag nanocubes and $HAuCl_4$.
- The Ag nanocubes serving as sacrificial templates can be readily prepared with a well-controlled size in a broad range of 13–200 nm through either the polyol method or seed-mediated growth.
- Gold nanocages possess a range of fascinating optical properties, including highly tunable LSPR peaks in the range of 600–1200 nm, large extinction cross-section and high ratio of absorption to scattering.

Advancement in optical imaging

- Gold nanocages can accumulate at the tumor site through both passive and active targeting, enabling their use as a novel class of theranostic agents for oncology.
- Gold nanocages can serve as superb contrast agents for both two-photon and three-photon luminescence microscopy, for both *in vitro* and *ex vivo* imaging.
- With large absorption cross-sections, Au nanocages can serve as a superb contrast agent for photoacoustic microscopy and photoacoustic tomography both *in vitro* and *in vivo*.
- With the incorporation of radioactive isotopes, Au nanocages can gain new optical property and serve as a tracer for cancer diagnostics with *in vivo* Cerenkov luminescence imaging.
- With $^{64}Cu^{2+}$ chelated onto the surface, the biodistribution profiles and tumor targeting capability of gold nanocages have been investigated by positron emission tomography.

Advancement in therapeutics

- Owing to their tunable localized surface plasmon resonance peaks and large absorption cross-sections, Au nanocages are efficient photothermal transducers and thus well-suited for *in vivo* photothermal therapy.
- The hollow interiors and porous walls of Au nanocages make them unique and ideal for drug encapsulation and delivery. Using Au nanocages as carriers, a variety of mechanisms have been explored to realize controlled release.

References

Papers of special note have been highlighted as: • of interest; •• of considerable interest

1 Dreaden EC, Alkilany AM, Huang XH, Murphy CJ, El-Sayed MA. The golden age: gold nanoparticle for biomedicine. *Chem. Soc. Rev.* 41(7), 2740–2779 (2012).

2 Chinen AB, Guan CM, Ferrer JR, Barnaby SN, Merkel TJ, Mirkin CA. Nanoparticle probes for the detection of cancer biomarkers, cells, and tissues by fluorescence. *Chem. Rev.* 115(19), 10530–10574 (2015).

3 He C, Liu D, Lin W. Nanomedicine applications of hybrid nanomaterials built from metal-ligand coordination bonds: nanoscale metal-organic frameworks and nanoscale coordination polymers. *Chem. Rev.* 115(19), 11079–11108 (2015).

4 Farokhzad OC, Langer R. Impact of nanotechnology on drug delivery. *ACS Nano* 3(1), 16–20 (2009).

5 Bertrand N, Wu J, Xu X, Kamaly N, Farokhzad OC. Cancer nanotechnology: the impact of passive and active targeting in the era of modern cancer biology. *Adv. Drug Deliv. Rev.* 66, 2–25 (2014).

6 Maeda H, Nakamura H, Fang J. The EPR effect for macromolecular drug delivery to solid tumors: Improvement of tumor uptake, lowering of systemic toxicity, and distinct tumor imaging *in vivo*. *Adv. Drug Deliv. Rev.* 65(1), 71–79 (2013).

7 Couvreur P. Nanoparticles in drug delivery: past, present and future. *Adv. Drug Deliv. Rev.* 65(1), 21–23 (2013).

8 Bao G, Mitragotri S, Tong S. Multifunctional nanoparticles for drug delivery and molecular imaging. *Annu. Rev. Biomed. Eng.* 15(1), 253–282 (2013).

9 Peer D, Karp JM, Hong S, Farokhzad OC, Margalit R, Langer R. Nanocarriers as an emerging platform for cancer therapy. *Nat. Nanotechnol.* 2(12), 751–760 (2007).

10 Sun T, Zhang SY, Pang B, Hyun DC, Yang M, Xia Y. Engineered nanoparticles for drug delivery in cancer therapy, *Angew. Chem. Int. Ed. Engl.* 53(46), 12320–12364 (2014).

11 Xia X, Xia Y. Gold nanocages as multifunctional materials for nanomedicine. *Front. Phys.* 9(3), 378–384 (2014).

12 Xia Y, Li W, Cobley CM *et al.* Gold nanocages: from synthesis to theranostic applications. *Acc. Chem. Res.* 44(10), 914–924 (2011).

13 Cobley CM, Chen J, Cho EC, Wang LV, Xia Y. Gold nanostructures: a class of multifunctional materials for biomedical applications. *Chem. Soc. Rev.* 40(1), 44–56 (2011).

14 Weissleder R. A clearer vision for *in vivo* imaging. *Nat. Biotechnol.* 19(4), 316–317 (2001).

15 Rodríguez-Fernández J, Pérez-Juste J, García de Abajo FJ, Liz-Marzán LM. Seeded growth of submicron Au colloids with quadrupole plasmon resonance modes. *Langmuir* 22(16), 7007–7010 (2006).

16 Skrabalak SE, Au L, Lu X, Li X, Xia Y. Gold nanocages for cancer detection and treatment. *Nanomedicine* 2(5), 657–668 (2007).

17 Sun Y, Mayers BT, Xia Y. Template-engaged replacement reaction: a one-step approach to the large-scale synthesis of metal nanostructures with hollow interiors. *Nano Lett.* 2(5), 481–485 (2002).

• **The first report on the use of galvanic replacement reaction at the nanometer scale with multiple-twined Ag nanoparticles serving as the sacrificial templates.**

18 Sun Y, Xia Y. Shape-controlled synthesis of gold and silver nanoparticles. *Science* 298(5601), 2176–2179 (2002).

•• **The first report on the synthesis of well-defined and controllable Au nanocages via the galvanic replacement reaction with single-crystal Ag nanocubes.**

19 Skrabalak SE, Chen J, Sun Y *et al.* Gold nanocages: synthesis, properties, and applications. *Acc. Chem. Res.* 41(12), 1587–1595 (2008).

20 Skrabalak SE, Au L, Li X, Xia Y. Facile synthesis of Ag nanocubes and Au nanocages. *Nat. Protocols* 2(9), 2182–2190 (2007).

21 Lu X, Au L, Mclellan J, Li Z-Y, Marquez M, Xia Y. Fabrication of cubic nanocages and nanoframes by dealloying Au/Ag alloy nanoboxes with an aqueous etchant based on $Fe(NO_3)_3$ or NH_4OH. *Nano Lett.* 7(6), 1764–1769 (2007).

22 Zhang Q, Cobley CM, Zeng J, Wen L-P, Chen J, Xia Y. Dissolving Ag from Au-Ag alloy nanoboxes with H_2O_2: a method for both tailoring the optical properties and measuring the H_2O_2 concentration. *J. Phys. Chem. C* 114(14), 6396–6400 (2010).

23 Yang X, Yang M, Pang B, Vara M, Xia Y. Gold nanomaterials at work in biomedicine. *Chem. Rev.* 115(19), 10410–10488 (2015).

• **A comprehensive review of the application of Au nanomaterials in biomedical research.**

24 Zeng J, Goldfeld D, Xia Y. A plasmon-assisted optofluidic (PAOF) system for measuring the photothermal conversion efficiencies of gold nanostructures and controlling an electrical switch. *Angew. Chem. Int. Ed. Engl.* 52(15), 4169–4173 (2013).

25 Cho EC, Kim C, Zhou F *et al.* Measuring the optical absorption cross sections of Au-Ag nanocages and Au nanorods by photoacoustic imaging. *J. Phys. Chem. C* 113(21), 9023–9028 (2009).

26 Hu M, Chen J, Li Z-Y *et al.* Gold nanostructures: engineering their plasmonic properties for biomedical applications. *Chem. Soc. Rev.* 35(11), 1084–1094 (2006).

27 Skrabalak SE, Wiley BJ, Kim M, Formo EV, Xia Y. On the polyol synthesis of silver nanostructures: glycolaldehyde as a reducing agent. *Nano Lett.* 8(7), 2077–2081 (2008).

28 Wiley B, Herricks T, Sun Y, Xia Y. Polyol synthesis of silver nanoparticles: use of chloride and oxygen to promote the formation of single-crystal, truncated cubes and tetrahedrons. *Nano Lett.* 4(9), 1733–1739 (2004).

29 Xia X, Zeng J, Oetjen LK, Li Q, Xia Y. Quantitative analysis of the role played by poly(vinylpyrrolidone) in seed-mediated growth of Ag nanocrystals. *J. Am. Chem. Soc.* 134(3), 1793–1801 (2011).

30 Siekkinen AR, Mclellan JM, Chen J, Xia Y. Rapid synthesis of small silver nanocubes by mediating polyol reduction with a trace amount of sodium sulfide or sodium hydrosulfide. *Chem. Phys. Lett.* 432(4–6), 491–496 (2006).

31 Zhang Q, Cobley C, Au L *et al.* Production of Ag nanocubes on a scale of 0.1 g per batch by protecting the NaHS-mediated polyol synthesis with argon. *ACS Appl. Mater. Interfaces* 1(9), 2044–2048 (2009).

32 Zhang Q, Li W, Wen L-P, Chen J, Xia Y. Facile synthesis of Ag nanocubes of 30 to 70 nm in edge length with CF_3COOAg as a precursor. *Chem. Eur. J.* 16(33), 10234–10239 (2010).

• **The most robust method for the synthesis of Ag nanocube.**

33 Chen J, Yang M, Zhang Q *et al.* Gold nanocages: a novel class of multifunctional nanomaterials for theranostic applications. *Adv. Funct. Mater.* 20(21), 3684–3694 (2010).

34 Wang Y, Zheng Y, Huang CZ, Xia Y. Synthesis of Ag nanocubes 18–32 nm in edge length: the effects of polyol on reduction kinetics, size control, and reproducibility. *J. Am. Chem. Soc.* 135(5), 1941–1951 (2013).

• **A recent report on the synthesis of Ag nanocubes as small as 18 nm in edge length and Au nanocages as small as 20 nm in edge length.**

35 Ruditskiy A, Xia Y. Toward the synthesis of sub-15 nm Ag nanocubes with sharp corners and edges: the roles of heterogeneous nucleation and surface capping. *J. Am. Chem. Soc.* 138(9), 3161–3167 (2016).

36 Au L, Zhang Q, Cobley CM *et al.* Quantifying the cellular uptake of antibody-conjugated Au nanocages by two-photon microscopy and inductively coupled plasma mass spectrometry. *ACS Nano* 4(1), 35–42 (2009).

37 Tong L, Cobley CM, Chen J, Xia Y, Cheng J-X. Bright three-photon luminescence from gold/silver alloyed nanostructures for bioimaging with negligible photothermal toxicity. *Angew. Chem. Int. Ed. Engl.* 49(20), 3485–3488 (2010).

38 Cho EC, Zhang Y, Cai X, Moran CM, Wang LV, Xia Y. Quantitative analysis of the fate of gold nanocages *in vitro* and *in vivo* after uptake by U87-MG tumor cells. *Angew. Chem. Int. Ed. Engl.* 52(4), 1152–1155 (2013).

39 Zhang YS, Wang Y, Wang L *et al.* Labeling human mesenchymal stem cells with gold nanocages for *in vitro* and *in vivo* tracking by two-photon microscopy and photoacoustic microscopy. *Theranostics* 3(8), 532–543 (2013).

40 Yang X, Skrabalak SE, Li Z-Y, Xia Y, Wang LV. Photoacoustic tomography of a rat cerebral cortex *in vivo* with Au nanocages as an optical contrast agent. *Nano Lett.* 7(12), 3798–3802 (2007).

41 Song KH, Kim C, Cobley CM, Xia Y, Wang LV. Near-infrared gold nanocages as a new class of tracers for photoacoustic sentinel lymph node mapping on a rat model. *Nano Lett.* 9(1), 183–188 (2009).

42 Kim C, Cho EC, Chen J *et al. In vivo* molecular photoacoustic tomography of melanomas targeted by boconjugated gold nanocages. *ACS Nano* 4(8), 4559–4564 (2010).

43 Wang Y, Liu Y, Luehmann H *et al.* Radioluminescent gold nanocages with controlled radioactivity for real-time *in vivo* imaging. *Nano Lett.* 13(2), 581–585 (2013).

•• **A report on the incorporation of ^{198}Au into the crystal lattice of Au nanocages. Most recently, the same approach has been employed by many groups for the labeling of nanostructures with radioactive isotopes for nuclear imaging.**

44 Wang H, Huff TB, Zweifel DA *et al. In vitro* and *in vivo* two-photon luminescence imaging of single gold nanorods. *Proc. Natl Acad. Sci. USA* 102(44), 15752–15756 (2005).

45 Wang T, Halaney D, Ho D, Feldman MD, Milner TE. Two-photon luminescence properties of gold nanorods. *Biomed. Opt. Express* 4(4), 584–595 (2013).

46 Mohamed MB, Volkov V, Link S, El-Sayed MA. The 'lightning' gold nanorods: fluorescence enhancement of over a million compared with the gold metal. *Chem. Phys. Lett.* 317(6), 517–523 (2000).

47 Mooradian A. Photoluminescence of metals. *Phys. Rev. Lett.* 22(5), 185–187 (1969).

48 Yang X, Stein EW, Ashkenazi S, Wang LV. Nanoparticles for photoacoustic imaging. *Wiley Interdiscip. Rev. Nanomed. Nanobiotechnol.* 1(4), 360–368 (2009).

49 Kim C, Favazza C, Wang LV. *In vivo* photoacoustic tomography of chemicals: high-resolution functional and molecular optical imaging at new depths. *Chem. Rev.* 110(5), 2756–2782 (2010).

50 Maslov K, Zhang HF, Hu S, Wang LV. Optical-resolution photoacoustic microscopy for *in vivo* imaging of single capillaries. *Opt. Lett.* 33(9), 929–931 (2008).

51 Gambhir SS. Molecular imaging of cancer with positron emission tomography. *Nat. Rev. Cancer* 2(9), 683–693 (2002).

52 Dobrucki LW, Sinusas AJ. PET and SPECT in cardiovascular molecular imaging. *Nat. Rev. Cardiol.* 7(1), 38–47 (2010).

53 Wang Y, Liu Y, Luehmann H *et al.* Evaluating the pharmacokinetics and *in vivo* cancer targeting capability of Au nanocages by positron emission tomography imaging. *ACS Nano* 6(7), 5880–5888 (2012).

54 Hirsch LR, Stafford RJ, Bankson JA *et al.* Nanoshell-mediated near-infrared thermal therapy of tumors under magnetic resonance guidance. *Proc. Natl Acad. Sci. USA* 100(23), 13549–13554 (2003).

55 Huang X, Jain P, El-Sayed IH, El-Sayed MA. Plasmonic photothermal therapy (PPTT) using gold nanoparticles. *Laser Med. Sci.* 23(3), 217–228 (2008).

56 Huang X, El-Sayed IH, Qian W, El-Sayed MA. Cancer cell imaging and photothermal therapy in the near-infrared region by using gold nanorods. *J. Am. Chem. Soc.* 128(6), 2115–2120 (2006).

57 Hasan W, Stender CL, Lee MH, Nehl CL, Lee J, Odom TW. Tailoring the structure of nanopyramids for optimal heat generation. *Nano Lett.* 9(4), 1555–1558 (2009).

58 Chen J, Wang D, Xi J *et al.* Immuno gold nanocages with tailored optical properties for targeted photothermal destruction of cancer cells. *Nano Lett.* 7(5), 1318–1322 (2007).

59 Wang Y, Black KCL, Luehmann H *et al.* Comparison study of gold nanohexapods, nanorods, and nanocages for photothermal cancer treatment. *ACS Nano* 7(3), 2068–2077 (2013).

60 Chen J, Saeki F, Wiley BJ *et al.* Gold nanocages: Bioconjugation and their potential use as optical imaging contrast agents. *Nano Lett.* 5(3), 473–477 (2005).

61 Chen J, Glaus C, Laforest R *et al.* Gold nanocages as photothermal transducers for cancer treatment. *Small* 6(7), 811–817 (2010).

62 Sperling RA, Parak WJ. Surface modification, functionalization and bioconjugation of colloidal inorganic nanoparticles. *Phil. Trans. R. Soc. A* 368(1915), 1333–1383 (2010).

63 Gref R, Lück M, Quellec P *et al.* 'Stealth' corona-core nanoparticles surface modified by polyethylene glycol (PEG), influences of the corona (PEG chain length and surface density) and of the core composition on phagocytic uptake and plasma protein adsorption. *Colloids Surf. B Biointerfaces* 18(3–4), 301–313 (2000).

64 Xia X, Yang M, Wang Y *et al.* Quantifying the coverage density of poly(ethylene glycol) chains on the surface of gold nanostructures. *ACS Nano* 6(1), 512–522 (2011).

65 Xia X, Yang M, Oetjen LK *et al.* An enzyme-sensitive probe for photoacoustic imaging and fluorescence detection of protease activity. *Nanoscale* 3(3), 950–953 (2011).

66 Radwan SH, Azzazy HM. Gold nanoparticles for molecular diagnostics. *Expert Rev. Mol. Diagn.* 9(5), 511–524 (2009).

67 Yavuz MS, Cheng Y, Chen J *et al.* Gold nanocages covered by smart polymers for controlled release with near-infrared light. *Nat. Mater.* 8(12), 935–939 (2009).

• **An early report on the controlled release of drugs from the interiors of Au nanocages through the use of smart polymer brushes as the 'gate keeper.'**

68 Moon GD, Choi SW, Cai X *et al.* A new theranostic system based on gold nanocages and phase-change materials with unique features for photoacoustic imaging and controlled release. *J. Am. Chem. Soc.* 133(13), 4762–4765 (2011).

69 Hoffman AS. Hydrogels for biomedical applications. *Adv. Drug Delivery Rev.* 54(1), 3–12 (2002).

70 Li W, Cai X, Kim C *et al.* Gold nanocages covered with thermally-responsive polymers for controlled release by high-intensity focused ultrasound. *Nanoscale* 3(4), 1724–1730 (2011).

71 Choi SW, Zhang Y, Xia Y. A temperature-sensitive drug release system based on phase-change materials. *Angew. Chem. Int. Ed. Engl.* 49(43), 7904–7908 (2010).